

Cite this: *J. Mater. Chem. C*, 2018,
6, 8135

Fabrication of a flexible and stretchable three-dimensional conductor based on Au–Ni@graphene coated polyurethane sponge by electroless plating†

Fei Han,^{‡,ab} Xingyu Su,^{‡,ac} Mingqi Huang,^a Jinhui Li,^{*ad} Yuan Zhang,^{ab} Songfang Zhao,^{id e} Feng Liu,^a Bo Zhang,^a Ying Wang,^{ab} Guoping Zhang,^{id *a} Rong Sun,^{id *a} and Ching-Ping Wong^f

Flexible and stretchable electronics, which could function properly under different deformations, have attracted extensive attention recently, due to their widespread application potential. Among them, flexible and stretchable conductors have played a significant role in bridging stretchable electronics (e.g., flexible strain sensors and stretchable energy storage devices) and measured targets (e.g., human motion detection and multifunctional output devices). Although various types of fabrication method for flexible conductors have been reported, the fabrication of stretchable conductors exhibiting stretchability, conductive stability, and durability remains a challenge. Here, we developed a flexible and stretchable three-dimensional (3D) conductor by the electroless plating technique. The prepared flexible and stretchable conductor combines two strengths including the excellent conductivity of 3D gold–nickel@graphene coated polyurethane sponge (Au–Ni@GPUS) conductive networks and the flexibility of casting encapsulated PDMS. The resistance of the conductor ranges from original 2.5 Ω to 4.0 Ω when the applied strain increased from 0% to 30% for the first stretching–releasing cycle. And after 1000 stretching–releasing cycles, the original resistance exhibited a small increase to 3.1 Ω , while the resistance under 30% applied strain was 6.0 Ω which well illustrates the conductive stability and durability. Besides, the resistance of the conductor is retained even after 1000 cycles of bending (the bending angle ranges from 0° to 180°) and twisting (the twisting angle ranges from 0° to 180°), confirming the excellent conductivity of the conductor. Additionally, the fabricated flexible and stretchable conductor has been successfully applied as a flexible interconnect of light-emitting diodes and a stretchable mobile phone charging interconnect.

Received 18th May 2018,
Accepted 5th July 2018

DOI: 10.1039/c8tc02413h

rsc.li/materials-c

Introduction

Flexible and stretchable conductors that feature both superior conductivity and large deformation stability have been widely used in a variety of applications, such as stretchable antennae,¹ stretchable transistors,² stretchable supercapacitors,^{3,4} electronic skins,⁵ and touch panels.^{6,7} In specific operating systems, the stretchable conductors are used as not only the vital flexible interconnects for the devices, but also the essential function segments for data output. With the purpose of fabricating high-performance stretchable conductors, several material strategies have been reported for developing nanomaterial-enabled highly conductive and stretchable conductors.^{8–10} One straightforward and effective method is to integrate highly conductive nanomaterials (e.g., graphene,^{11–13} carbon nanotubes (CNTs)/fibers,^{14–16} and metal nanowires/nanoparticles^{17–19}) with elastomeric materials (e.g., polydimethylsiloxane (PDMS)),^{20,21}

^a Guangdong Provincial Key Laboratory of Materials for High Density Electronic Packaging, Shenzhen Institutes of Advanced Technology, Chinese Academy of Sciences, Shenzhen 518055, China. E-mail: gp.zhang@siat.ac.cn, rong.sun@siat.ac.cn

^b Department of Nano Science and Technology Institute, University of Science and Technology of China, Suzhou 215123, China

^c School of Chemical Engineering, China University of Petroleum, Beijing 102249, China

^d Department of Materials Science and Engineering, City University of Hong Kong, 83 Tat Chee Avenue, Kowloon, Hong Kong 999077, China

^e School of Material Science and Engineering, University of Jinan, Jinan 250022, Shandong, China

^f School of Materials Science and Engineering, Georgia Institute of Technology, 771 Ferst Drive, Atlanta, Georgia 30332, USA

† Electronic supplementary information (ESI) available. See DOI: 10.1039/c8tc02413h

‡ These authors contributed equally to this work.

polyurethane (PU),^{22,23} spun poly(styrene-*block*-butadiene-*block*-styrene) (SBS),^{2,24} and Ecoflex^{25,26}, and these nanomaterials are commonly designed on top of or are embedded inside the elastomeric materials to form composites. However, in order to maintain an ingenious balance between mechanical deformability and electrical performances, the loading of conductive fillers and elastomeric materials should be controlled strictly during the fabrication process. For example, the fabrication of a CNT-VHB 4905 composite conductive thin film by using a spraying method through shadow masks has been reported.²⁷ Although the fabrication process was simple and economical, the super-linear increased electrical performance with the applied strain of the obtained material ($10^7 \Omega$ at 700% strain) affected its application under various conditions which requires conductive stability. Moreover, due to the sliding between conductive nanomaterials when an external strain is applied, the effective contact area of electrical conduction decreased which directly caused a decrease in the conductivity of the conductors.

To overcome the abovementioned problems, several solutions have been introduced in the stretchable structures. For example, periodic “wavy” microstructures on elastomeric substrates by mechanical buckling, which are achieved through the pre-straining and release process, make the conductive nanomaterials acquire buckling behaviour and wide-range stretchability.^{28–30} Because the periodic “wavy” microstructures can increase the buckling wavelength and decrease the buckling amplitude when an external strain is applied, the electric resistance remains unchanged. However, the transfer process of the complicated nanomaterials is not suitable for large-scale manufacturing processes. Other stretchable microstructures, such as spring structures³¹ and net-shaped structures,^{32,33} have also been developed by using 1D nanomaterials (*e.g.*, CNTs,³⁴ and metal nanowires²³) and different fabrication technologies (*e.g.*, template methods,³⁵ electrospinning,³⁶ and dispersing¹⁶). Upon stretching, these structures can accommodate the applied strain by changing the shape or sliding and rotating inside themselves.⁸ Although the stretchable conductors fabricated using those designed microstructures exhibit some applications, the required advantages of high stretchability and stability still make their mass production and pervasive application difficult. For example, a CNT/PDMS based stretchable conductor has been fabricated by stretching–release–buckling strategies which showed high stretchability up to 100% of its original length.³⁷ However, the relatively poor electrical properties which are stable at 3.5 k Ω within 100% strain limited its further application.

Compared with the aforementioned stretchable patterns, three-dimensional (3D) conductive network structures have drawn significant attention in recent years because these materials can be fabricated by a lower cost manufacturing procedure, possess mechanical durability, electrical stability, and large-scale manufacturing applications.^{38–40} Among them, 3D graphene-based networks have been further studied due to their good electrical conductivity, large specific surface area, and excellent mechanical performance. But some of the graphene fabrication methods, such as chemical vapor deposition (CVD) on

copper/nickel foam skeletons^{41,42} and hydrothermal reduction of graphene oxides,^{43,44} have limitations and are time consuming. For instance, three-dimensional porous stretchable and conductive polymer composites based on graphene networks grown by CVD and PEDOT:PSS coating have been reported which exhibited high conductive performance.³⁸ But their complicated and costly fabrication method makes their mass production and pervasive application difficult. We recently reported that 3D graphene sponge fabricated by a repeated absorption–reduction process is an excellent substrate material with relatively good conductivity and mechanical performance.⁴⁵ The 3D graphene sponge was used for the preparation of crack-based flexible strain sensors through the electrodeposition method. However, it was not appropriate for stretchable conductors due to the wide-range of resistance variations when stretched caused by the derived micro-cracks. Therefore, we chose another method for the fabrication of a 3D graphene sponge based stretchable conductor. Electroless plating, a simple, energy conserving, environmentally friendly and economical surface treatment technology, has been widely used in different applications, such as corrosion protection,⁴⁶ wear-resistance protection,⁴⁷ and conductive coatings.⁴⁸ Furthermore, compared with the electrodeposition method, no microcracks are generated during electroless plating,⁴⁹ therefore the even coating with excellent conductivity by electroless gold plating fits well with the fabrication of conductors.

Here, we demonstrated the fabrication of a flexible and stretchable 3D conductor based on our previous work on 3D graphene sponge and the advantages of electroless gold plating. The fabricated conductor exhibited excellent flexibility and conductive stability within 30% strain. Moreover, 1000 cycles of stretching–releasing (0% to 30% strain), bending–releasing (the bending angle ranges from 0° to 180°) and twisting–releasing (the twisting angle ranges from 0° to 180°), respectively, confirmed the excellent stable conductivity of the conductor. The principles of this fabrication method and the work mechanism of the conductor have been also proposed. Additionally, the fabricated flexible and stretchable conductor has been successfully applied as a flexible interconnect of light-emitting diodes (LED) and a stretchable mobile phone charging interconnect, indicating their tremendous potential in the field of flexible electronics.

Results and discussion

The fabrication process is schematically illustrated in Fig. 1. Briefly, a piece of commercial polyurethane sponge (PUS) was coated with graphene oxide through the full immersion method in a vacuum, followed by reduction with hot hydroiodic acid (HI), forming a graphene coated PU sponge (GPUS). The above process was repeated for four cycles and a multilayer graphene coated PU sponge with good conductivity was obtained. After that, a thin layer of nickel coated GPUS (Ni@GPUS) was processed by electroless plating. The nickel layer on the Ni@GPUS material was then substituted by a gold layer through electroless plating. The thickness of the gold layer

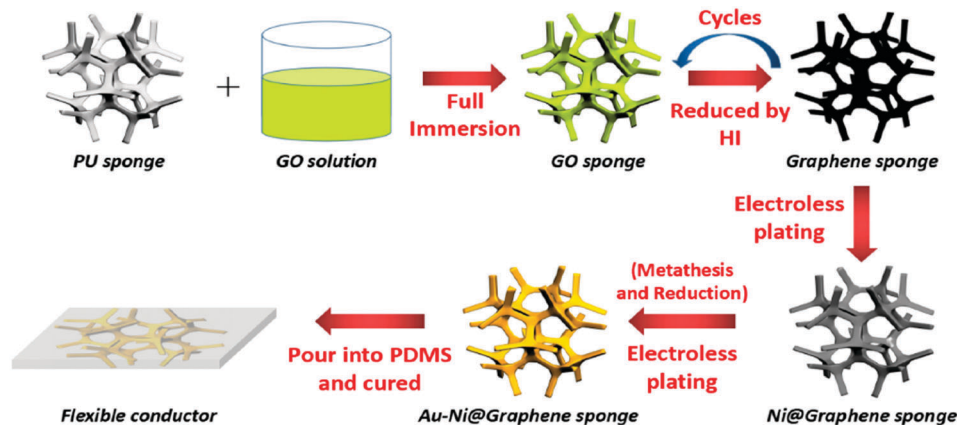


Fig. 1 A schematic of the fabrication process of the Au–Ni@graphene flexible conductor.

was increased by the reduction reaction during electroless plating and a 3D Au–Ni@GPUS conductive material was obtained. Finally, the Au–Ni@GPUS was poured into PDMS in a vacuum environment and then cured together, resulting in a flexible and stretchable conductor. The optical images of the as-prepared PUS, GPUS, Au–Ni@GPUS, and the flexible conductor are exhibited in Fig. S1 (ESI[†]).

Some details on the fabrication process of a flexible conductor need to be discussed here. First, before electroless nickel plating, the GPUS should be pre-activated by the sandwich structure (Fig. S2a, ESI[†]) designed by us. The GPUS was placed between two copper foils as a whole, followed by pre-activation treatment in the PdSO₄ solution. There are two reasons for GPUS to have a designed sandwich structure. First, on the one hand, the Pd crystal nucleus is an important catalyst that allows the next electroless nickel plating reaction to take place, so the generated Pd crystal nucleus in the GPUS skeleton needs the assistance of copper foil to enable the Pd²⁺ + Cu → Pd + Cu²⁺ reaction to proceed. On the other hand, the copper foil sandwich structure makes the GPUS fixed and preserves its shape during the next electroless nickel plating process. Second, the principle of electroless nickel plating is the Ni²⁺ + H₂PO₂[−] + H₂O → Ni + H₂PO₃[−] + 2H⁺ and 6H₂PO₂[−] + 2H⁺ → 2P + 4H₂PO₃[−] + 3H₂ reactions that take place by the catalysis of the Pd crystal nucleus to H₂PO₂[−].⁵⁰ And the thinner nickel layer played the role of the seed in the growth of Au in the next electroless gold plating. Third, the gold layer is grown in two steps: the replacement reaction and the reduction reaction, and the chemical reaction equations are Ni + 2Au⁺ → Ni²⁺ + Au and C₆H₈O₆ + 2Au⁺ → 2Au + C₆H₆O₆ + 2H⁺, respectively.^{51,52} The replacement reaction decreases the thickness of the nickel layer and it would shutoff when the nickel surface was completely covered with the gold. And the subsequent reduction reaction was triggered by the catalysis of gold to L-ascorbic acid which would thicken the gold layer. Fourth, the good property of PDMS ensured the flexibility and stretchability of the conductor.

Malleability is a significant feature of metals. In this work, we chose Au–Ni as the materials for excellent conductivity due to the better malleability of gold than nickel while the nickel

layer was used as the seed layer for the development of the gold layer.^{53–55} The different degree of metal bonds corresponds to different malleability. Because of the relatively larger radius of the metal atoms, the number of valence electrons is relatively smaller. So, the electrons easily break away from metal atoms and become free electrons (also called “delocalized electrons”) which no longer belong to any atom. When an external force is applied, positive metal ions glide without breaking because of the existence of free electrons around them, resulting in good malleability of metals.

Fig. 2a shows the SEM image of the original structure of the commercial PUS. The sizes of porous structures range from 100 to 300 μm and these kinds of structures are beneficial to the next absorption–reduction process. The surfaces of the PUS structures are gradually coated with wrinkled multilayer graphene with increasing absorption–reduction cycles as indicated in Fig. 2b, c and d (1 cycle, 3 and 5 cycles, respectively). The conductivity of the evolved GPUS improved simultaneously as the absorption–reduction cycles increased,⁴⁵ and the GPUS with good electrical conductivity is a good basis material for the next electroless plating procedure. Fig. 2e illustrates the SEM image of the surface of Ni@GPUS fabricated by electroless nickel plating, and it is observed that the nickel film covers the GPUS material evenly. Different from our previous work on the synthesis of nickel based strain sensors by electrodeposition, no microcracks were observed on the surfaces of the Ni@GPUS sample when using the electroless nickel plating method, which could afford uniformity, compactness and consistency features. Besides, the nonoccurrence of the point discharge phenomenon during the electroless nickel plating process was also another important difference between the electrodeposition method and the electroless nickel plating process. And the obtained Ni@GPUS sample without microcracks is propitious for the fabrication of a flexible conductor with stable conductivity. The SEM image of Au–Ni@GPUS is shown in Fig. 2f, which reveals that the Ni@GPUS sample was completely covered with gold by two electroless gold plating processes. The Au–Ni@GPUS composites exhibit excellent conductivity and relatively good flexibility which are encouraging features for the flexible and stretchable conductor.

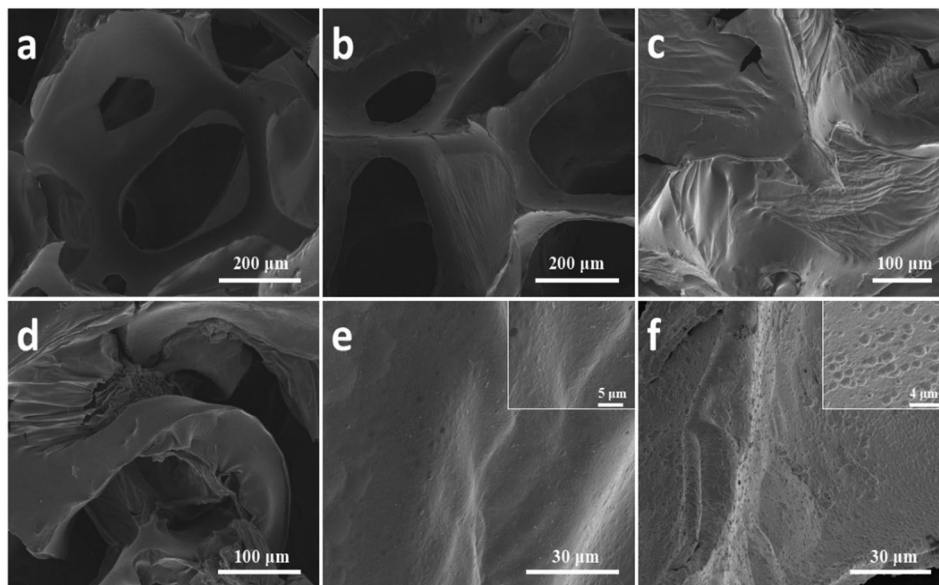


Fig. 2 (a) SEM image of the original PUS. (b–d) SEM images of GPUS with different absorption–reduction cycles (1 cycle, 3 and 5 cycles, respectively). (e) SEM image of the Ni@GPUS sample. (f) The surface SEM image of the Au–Ni@GPUS sample.

The X-ray diffraction (XRD) patterns of graphene oxide coated PUS (GO-PUS) and GPUS are shown in Fig. 3a. GO-PUS has a dominant peak (001) centered at $2\theta = 10.98^\circ$. After the absorption–reduction process for four cycles, the GO was completely reduced by a hot HI solution, and a broad peak (002) centered at $2\theta = 23.86^\circ$ was observed which indicates the presence of the graphene sheets of the prepared GPUS sample.⁵⁶ The XRD patterns of Ni@GPUS and Au–Ni@GPUS are displayed in Fig. 3b. Because the nickel–phosphorus (Ni–P) amorphous state materials were generated during the electroless nickel plating process, the characteristic peak at $2\theta = 44.97^\circ$ corresponds to the broad peak.⁵⁷ And this result is also

consistent with the Energy Dispersive Spectroscopy (EDS) analysis as shown in Fig. S3a (ESI[†]). The diffraction peaks for the Au–Ni@GPUS sample observed at $2\theta = 38.10^\circ$, 44.35° , 64.46° , and 77.60° correspond to (111), (200), (220), and (311) characteristic planes which are assigned to Au, respectively.⁵⁸ Besides, the EDS analysis of Au–Ni@GPUS (Fig. S3b, ESI[†]) also demonstrates the Au coated sample by electroless gold plating. To clarify the thickness of Au and Ni layers, cross section mapping was introduced to measure the two different layers. From Fig. 3c, it can be seen that the thickness of the Au layer is 315–350 nm and that of the Ni layer is 250–275 nm. Because the Ni layer was displaced by Au and further electroless plating thickened the Au layer, the Au layer became thicker than the Ni layer which is beneficial for the flexible conductor as Au has excellent malleability. Furthermore, in order to verify the abovementioned principle, we tested the electrical stability of Ni@GPUS and Au–Ni@GPUS based flexible conductors, respectively, which were encapsulated by PDMS in equivalent situations. From Fig. 3d, it is observed that the electrical conductivity of the Au–Ni@GPUS sample remains stable when the strain increased from 0% to 30%, while that of the Ni@GPUS sample varies significantly. Therefore, Au–Ni@GPUS is an appropriate material for the fabrication of a flexible conductor.

To further testify the properties of Au–Ni@GPUS as a flexible and stretchable conductor, we studied the resistance variations of the Au–Ni@GPUS flexible conductor in different deformation states, such as stretching, bending, and twisting. Here, R_0 is the initial resistance of the Au–Ni@GPUS flexible conductor and $\Delta R/R_0$ represents the resistance variations as a function of different applied tensile strains and bending/twisting degrees. The schematic diagram of a tension measurement setup is illustrated in Fig. 4a, and the electrical performance of the

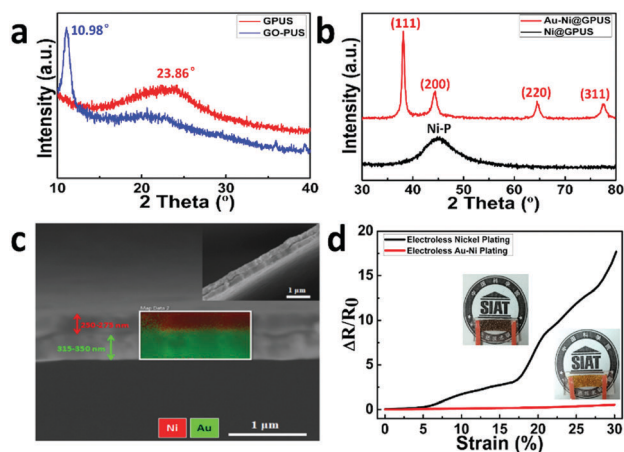


Fig. 3 (a) XRD patterns of the GPUS and GO-PUS samples. (b) XRD patterns of the Ni@GPUS and Au–Ni@GPUS samples. (c) The mapping of the cross section of the Au–Ni@GPUS sample. (d) The electrical performance of the Ni@GPUS and Au–Ni@GPUS based flexible conductor samples when stretched; the inset shows the images of the two samples.

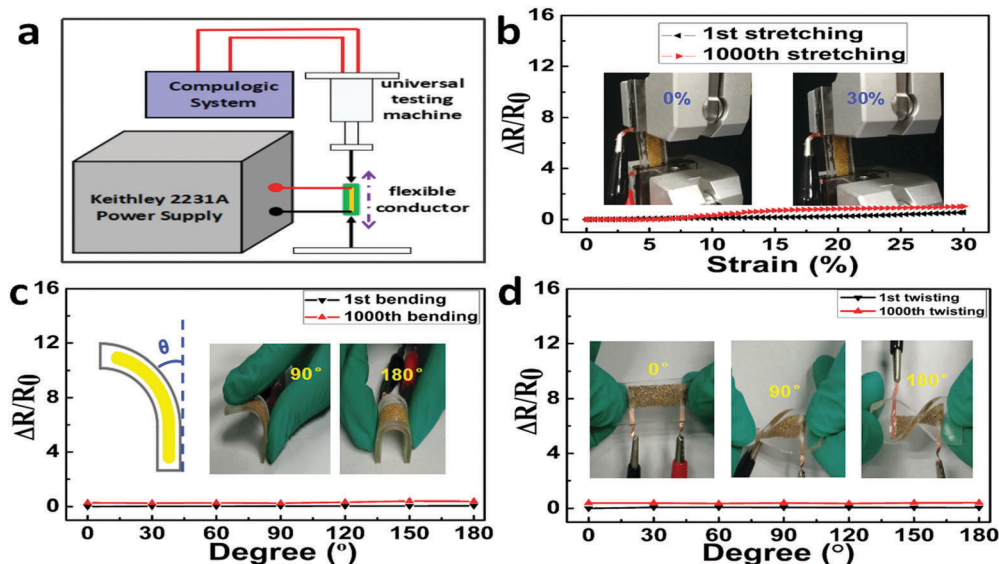


Fig. 4 (a) A schematic of the tension measurement setup. (b) The relative resistance changes of the Au–Ni@GPUS flexible conductor during the 1st stretching and 1000th stretching process; the inset images show the flexible conductor under 0% strain and 30% strain. (c) The relative resistance variations of the Au–Ni@GPUS flexible conductor during the 1st bending and 1000th bending process; the inset images are the definition of bending degree, 90° and 180° pictures, respectively. (d) The relative resistance changes of flexible conductors during the 1st twisting and 1000th twisting process; the inset images show the flexible conductor under different twisting degrees (0°, 90° and 180°, respectively).

Au–Ni@GPUS flexible conductor was measured using a universal testing machine and the output signals were processed by the compulogic system. As shown in Fig. 4b, the $\Delta R/R_0$ remains stable in the first stretching process when an external tension is applied from 0% to 30%. After 1000 stretching–releasing cycles, the $\Delta R/R_0$ still remains stable within 10% strain and slightly increases from 10% strain to 30% strain which still meets the requirements of a flexible conductor.

Besides, when the Au–Ni@GPUS flexible conductor was bent from 0° to 180° for 1000 cycles (the definition of the bending degree is shown in the inset graph in Fig. 4c), the invariability of $\Delta R/R_0$ demonstrates the electrical stability of the conductor. Furthermore, the twisting states had virtually no effects on the electrical stability of the Au–Ni@GPUS flexible conductor even after 1000 twisting–releasing cycles under 0° to 180° twisting degrees (Fig. 4d). There are two factors that contribute to the

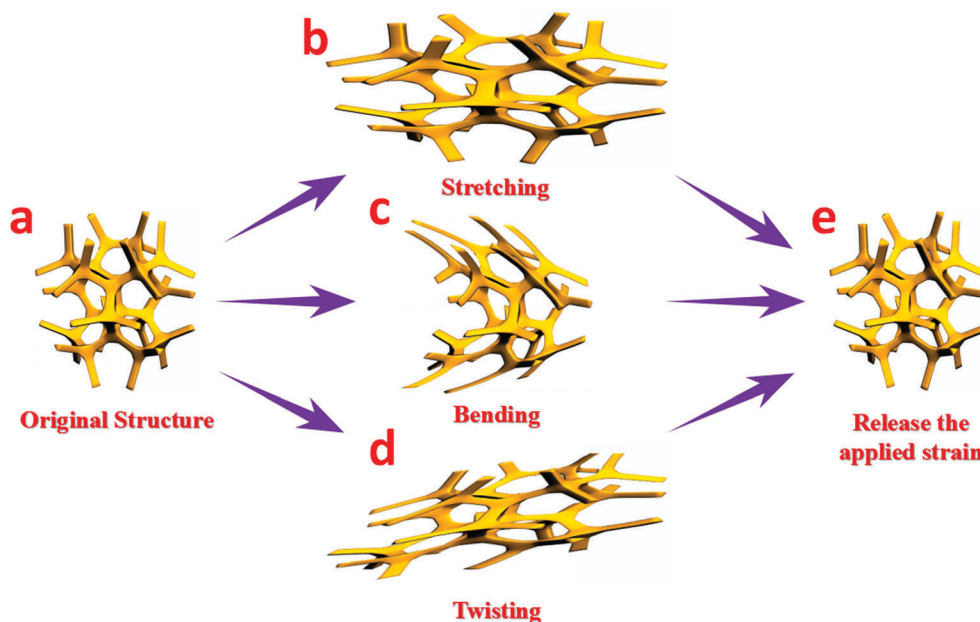


Fig. 5 Work mechanisms of the Au–Ni@graphene flexible conductor under different deformations. (a and e) The original structure and the structure when the applied strain released, respectively. (b–d) The structure when stretching, bending and twisting, respectively.

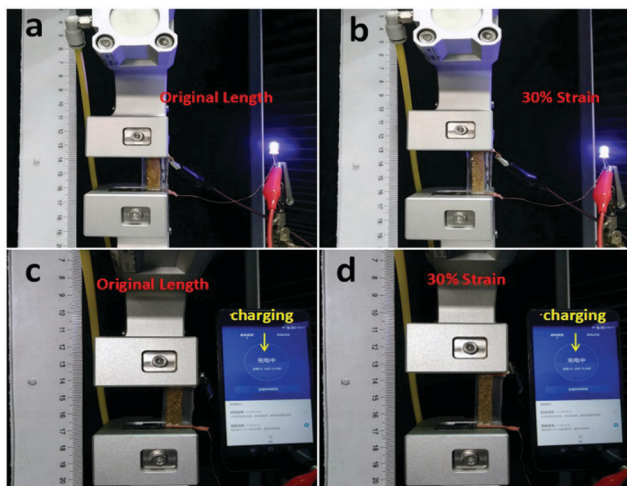


Fig. 6 (a and b) Optical images of the LED lights under original length and 30% strain of the Au-Ni@GPUS flexible conductor. (c and d) Optical images of the Au-Ni@GPUS flexible conductor as a charging interconnect under 0% and 30% strain.

good performance of the Au-Ni@GPUS flexible conductor. First, the 3D Au-Ni@GPUS conductive material with excellent conductivity possesses good malleability and relative flexibility due to the coated Au layer and the PUS substrate which all endow the flexible conductor with the ability to adapt to the deformations when a strain is applied. Second, PDMS integrated with the Au-Ni@GPUS conductive material has become a whole flexible conductor material because the cast and cured PDMS under vacuum conditions permeated every hole of the porous structures. Therefore, the good stretchability and resilience properties of PDMS have transferred to the Au-Ni@GPUS flexible conductor which ensured the electrical stability of the conductor under different applied strains.

The excellent electrical stability of the Au-Ni@GPUS flexible conductor in different deformation states shows its great application potential in flexible and stretchable electronic devices.

A schematic diagram of the work mechanism of the Au-Ni@GPUS flexible conductor during different deformations is shown in Fig. 5. The original Au-Ni@GPUS material possesses a 3D porous structure coated Au layer as the outermost layer (Fig. 5a). Because the encapsulation process was carried out in a vacuum, the PDMS permeated every pore of the structure and was cured in a vacuum oven. When the PDMS was cured, the PDMS coated every skeleton of the Au-Ni@GPUS material and ensured the stability of the material. In addition, PDMS also provides vital features to the conductor, such as high flexibility and stretchability. When an external strain is applied, the Au-Ni@GPUS flexible conductor was in stretching, bending and twisting states, respectively (Fig. 5b–d). The structure of the Au-Ni@GPUS flexible conductor bend to the strain direction according to different deformations. Here, there are two necessary factors that contribute to the electrical conductivity and stability during the three deformations. First, the good malleability of Au is an important element to maintain the congruent deformation of the 3D Au-Ni@GPUS material with applied strain. And this can also be confirmed from Fig. 3d, and the relative electrical signal of the Au-Ni@GPUS conductor almost remained stable during the stretching process compared with that of the Ni@GPUS material. Second, the entire Au-Ni@GPUS material is filled with cured PDMS, providing excellent stability and flexibility to the entire material. The structure of the Au-Ni@GPUS conductor deformed with PDMS when external strain applied while without destructive structure happened. Different from our previous work, no microcracks were generated when using the electroless plating method due to its good homogeneity, uniformity and simultaneity and this also ensures stable conductivity during the deformation process. Finally, when

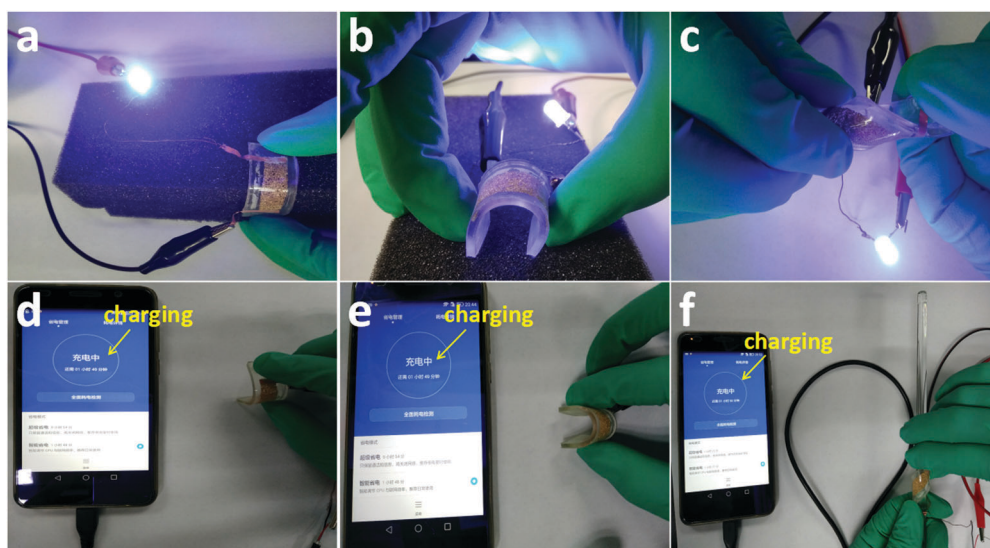


Fig. 7 (a–c) Optical images of the Au-Ni@GPUS flexible conductor as a stretchable LED interconnect when bending at 90° and 180°, and twisting at 180°, respectively (the applied voltage was 2V). (d–f) Optical images of the Au-Ni@GPUS flexible conductor as a stretchable smart cellphone charging interconnect when bending at 90° and 180°, and twisting at 180°, respectively (the applied voltage was 2V).

the applied strain is released as in Fig. 5e, the structure of the Au–Ni@GPUS material restored to its initial state.

The practical applications of the Au–Ni@GPUS flexible conductor were also studied, as shown in Fig. 6. A light-emitting diode (LED) lamp was installed in the conductive path which is connected to the Au–Ni@GPUS flexible conductor. The LED lamp was turned on when the Au–Ni@GPUS flexible conductor remained in its original length (without strain) and the applied voltage was 2V (Fig. 6a), and it still maintained its brightness when the applied strain was up to 30% (Fig. 6b). The dynamic circulatory testing video of the LED lamp is shown in the ESI,† Video S1. With the rapid development of smart cellphones, there is a great demand for adaptive flexible and stretchable charging interconnects. Therefore, here, we demonstrated the embedded Au–Ni@GPUS flexible conductor as a part of charging interconnects and charging smart cellphones when stretched. And the designed circuit diagram is shown in Fig. S2b (ESI†). From Fig. 6c, it can be seen that the smart cellphone was charging normally when the Au–Ni@GPUS flexible conductor in its original length. As the applied strain increased to 30% as in Fig. 6d, the charging status remained stable without any variation which manifested the stable performance of the Au–Ni@GPUS flexible conductor as a flexible and stretchable charging interconnect for smart devices. Besides, for a further explanation of the stability of the flexible conductor, the video of several stretching–releasing cycles when charging a smart cellphone is shown in the ESI,† Video S2.

We also investigated the LED lamp turning on test and smart cellphone charging test when the Au–Ni@GPUS flexible conductor was kept at different bending and twisting degrees, and the Au–Ni@GPUS flexible conductor was connected in series in the closed circuit. From Fig. 7a and b, we can see that the LED lamp turned on when the Au–Ni@GPUS flexible conductor was bent at 90° and 180°. When it was twisted at 180° (Fig. 7c), the LED lamp still remains switched on without any fading of brightness. Similarly, the successful realization of smart cellphone charging when the Au–Ni@GPUS flexible conductor is in different deformation states (bending degrees of 90° and 180°, and a twisting degree of 180°) is shown in Fig. 7d–f, respectively. Through a series of application tests, it has been proved that the fabricated Au–Ni@GPUS flexible conductor could be used to connect rigid device components as a stretchable interconnect. Furthermore, the high electrical conductivity and excellent mechanical stability give the Au–Ni@GPUS flexible conductor great application potential when integrated with other flexible devices.

Conclusions

In conclusion, a flexible and stretchable 3D conductor has been developed by the electroless plating technique. Au–Ni@graphene coated PU sponge serves as a skeleton structure to interconnect into a 3D flexible network, leading to high electrical conductivity and excellent flexibility. The Au–Ni@GPUS flexible conductor exhibits a 3D porous microstructure, good stretchability and

durability, and excellent electrical properties, resulting in its huge potential for applications such as stretchable interconnects and flexible charging interconnects. It is believed that the outstanding electromechanical properties of the flexible conductor are due to the PDMS assisted and robust 3D networks of the Au–Ni@GPUS materials that provide a stable and interconnected conductive pathway. Besides, the electroless plating technique is a simple, scalable, and low-cost strategy, which is beneficial for the large-scale production of this kind of flexible conductor. We believe that such a 3D flexible and stretchable conductor holds great application potential in stretchable next-generation electronics.

Methods

Materials

Commercial polyurethane sponges (PUS, one millimetre in thickness) were purchased from Chengxing Hong Co., Shenzhen, China. Graphene oxide (GO) and NiSO₄·6H₂O were purchased from Sinopharm Chemical Reagent Co., Ltd, China. Na₂S₂O₈, PdSO₄, H₂SO₄, NaH₂PO₂·H₂O, sodium acetate trihydrate, L-ascorbic acid and sodium citrate were purchased from Aladdin Co., Shanghai, China. Na₃Au(SO₃)₂ was purchased from Changzhou Chemical Research Institute Co., Ltd, China. Na₂SO₃, N(CH₂PO₃H₂)₃ and Na₃C₆H₅O₇·2H₂O were purchased from Wei Lian Fine Chemical Co., Ltd, China. PDMS prepolymer and the curing agent were supplied as two-part liquid component kits from Dow Corning (Sylgard 184). Polytetrafluoroethylene moulds were purchased from Shenzhen Huaxin Plastic Products Co., Ltd, China.

Preparation of the Au–Ni@graphene coated PUS (Au–Ni@GPUS) material

Graphene coated PUS (GPUS) was synthesized by the repeated absorption–reduction method according to our previous report.⁴³ The obtained GPUS was cut into pieces 40 mm long and 10 mm wide. Before electroless plating, the GPUS was placed between two copper foils forming a sandwich structure. Then it was micro-etched in an acid solution (30 g L⁻¹ Na₂S₂O₈, pH = 1.5, 5 min) and activated in an activating solution (20 ppm PdSO₄ and 13 mL L⁻¹ H₂SO₄) for 10 min. After each of these pre-treatment steps, the GPUS was washed with deionized water. The GPUS was immersed in the electroless nickel plating solution (25 g L⁻¹ NiSO₄·6H₂O, 30 g L⁻¹ NaH₂PO₂·H₂O, 10 g L⁻¹ sodium citrate, 30 g L⁻¹ sodium acetate trihydrate, pH = 4.6, 80 °C, 5 min) to perform electroless Ni deposition. Ni coated GPUS (Ni@GPUS) was obtained and washed with deionized water. Then the Ni@GPUS was immersed in an Au immersion bath (2 g L⁻¹ Na₃Au(SO₃)₂, 38 g L⁻¹ Na₂SO₃, 20 g L⁻¹ N(CH₂PO₃H₂)₃, pH = 7.0, 80 °C, 20 min), in which the replacement reaction takes place. Finally, the Au coated Ni@GPUS was immersed in the electroless Au plating solution (2 g L⁻¹ Na₃Au(SO₃)₂, 20 g L⁻¹ Na₂SO₃, 10 g L⁻¹ Na₃C₆H₅O₇·2H₂O, 1 g L⁻¹ C₆H₈O₆, pH = 6.9, 50 °C, 30 min) to perform electroless Au deposition, during which the reduction reaction takes place

to get a thicker gold layer. After being washed with deionized water and dried, gold and nickel coated GPUS (Au–Ni@GPUS) was obtained. During the electroless procedure, the plating solutions were agitated using rotating magnetic stirrer.

Preparation of the Au–Ni@GPUS flexible conductor

A piece of Au–Ni@GPUS 40 mm long and 10 mm wide was used for the fabrication of the flexible conductor. A slice of Au–Ni@GPUS was first connected with copper wires using silver paste and cured at 80 °C for 1 h. After the conductive silver adhesives were completely cured, the Au–Ni@GPUS was infiltrated with PDMS in a 10 : 1 (base/curing agent) ratio in a polytetrafluoroethylene (PTFE) mold and degassed in a vacuum oven for 1 h followed by curing at 80 °C for 3 h. After curing PDMS, a 3D Au–Ni@GPUS flexible conductor was obtained.

Conflicts of interest

There are no conflicts to declare.

Acknowledgements

This work was financially supported by the Guangdong and Shenzhen Innovative Research Team Program (No. 2011D052, KYPT20121228160843692), NSFC-Guangdong Jointed Funding (U1601202), NSFC-Shenzhen Robot Jointed Funding (U1613215), the Natural Science Foundation of China (21601065), R&D Funds for basic Research Program of Shenzhen (Grant No. JCYJ20150401145529012), the Key Deployment Project of Chinese Academy of Sciences (Grant No. KFZD-SW-202), the National and Local Joint Engineering Laboratory of Advanced Electronic Packaging Materials (Shenzhen Development and Reform Committee 2017-934), the Leading Scientific Research Project of Chinese Academy of Sciences (QYZDY-SSW-JSC010), and the Guangdong Provincial Key Laboratory (2014B030301014).

Notes and references

- M. Park, J. Im, M. Shin, Y. Min, J. Park, H. Cho, S. Park, M. B. Shim, S. Jeon, D. Y. Chung, J. Bae, J. Park, U. Jeong and K. Kim, *Nat. Nanotechnol.*, 2012, **7**, 803.
- M. Shin, J. H. Song, G. H. Lim, B. Lim, J. J. Park and U. Jeong, *Adv. Mater.*, 2014, **26**, 3706.
- Z. Niu, H. Dong, B. Zhu, J. Li, H. H. Hng, W. Zhou, X. Chen and S. Xie, *Adv. Mater.*, 2013, **25**, 1058.
- C. Yu, C. Masarapu, J. Rong, B. Wei and H. Jiang, *Adv. Mater.*, 2009, **21**, 4793.
- M. Chen, L. Zhang, S. Duan, S. Jing, H. Jiang and C. Li, *Adv. Funct. Mater.*, 2014, **24**, 7548.
- S. Han, S. Hong, J. Ham, J. Yeo, J. Lee, B. Kang, P. Lee, J. Kwon, S. S. Lee, M. Y. Yang and S. H. Ko, *Adv. Mater.*, 2014, **26**, 5808.
- J. Lee, P. Lee, H. B. Lee, S. Hong, I. Lee, J. Yeo, S. S. Lee, T. S. Kim, D. Lee and S. H. Ko, *Adv. Funct. Mater.*, 2013, **23**, 4171.
- S. Yao and Y. Zhu, *Adv. Mater.*, 2015, **27**, 1480.
- S. Zhao, J. Li, D. Cao, G. Zhang, J. Li, K. Li, Y. Yang, W. Wang, Y. Jin and R. Sun, *ACS Appl. Mater. Interfaces*, 2017, **9**, 12147.
- D. Langley, G. Giusti, C. Mayousse, C. Celle, D. Bellet and J. P. Simonato, *Nanotechnology*, 2013, **24**, 452001.
- J. Zang, S. Ryu, N. Pugno, Q. Wang, Q. Tu, M. J. Buehler and X. Zhao, *Nat. Mater.*, 2013, **12**, 321.
- Z. Chen, W. Ren, L. Gao, B. Liu, S. Pei and H. M. Cheng, *Nat. Mater.*, 2011, **10**, 424.
- K. S. Kim, Y. Zhao, H. Jang, S. Y. Lee, J. M. Kim, K. S. Kim, J. H. Ahn, P. Kim, J. Y. Choi and B. H. Hong, *Nature*, 2009, **457**, 706.
- T. Sekitani, H. Nakajima, H. Maeda, T. Fukushima, T. Aida, K. Hata and T. Someya, *Nat. Mater.*, 2009, **8**, 494.
- T. Sekitani, Y. Noguchi, K. Hata, T. Fukushima, T. Aida and T. Someya, *Science*, 2008, **321**, 1468.
- L. Hu, W. Yuan, P. Brochu, G. Gruner and Q. Pei, *Appl. Phys. Lett.*, 2009, **94**, 161108.
- W. Hu, X. Niu, R. Zhao and Q. Pei, *Appl. Phys. Lett.*, 2013, **102**, 38.
- D. C. Hyun, M. Park, C. Park, B. Kim, Y. Xia, J. H. Hur, J. M. Kim, J. J. Park and U. Jeong, *Adv. Mater.*, 2011, **23**, 2946.
- W. Huang, J. Li, S. Zhao, F. Han, G. Zhang, R. Sun and C. P. Wong, *Compos. Sci. Technol.*, 2017, **146**, 169.
- F. Xu, X. Wang, Y. Zhu and Y. Zhu, *Adv. Funct. Mater.*, 2012, **22**, 1279.
- Y. Y. Huang and E. M. Terentjev, *Adv. Funct. Mater.*, 2010, **20**, 4062.
- Y. Kim, J. Zhu, B. Yeom, M. Di Prima, X. Su, J. G. Kim, S. J. Yoo, C. Uher and N. A. Kotov, *Nature*, 2013, **500**, 59.
- W. Hu, R. Wang, Y. Lu and Q. Pei, *J. Mater. Chem. C*, 2014, **2**, 1298.
- M. Park, J. Im, M. Shin, Y. Min, J. Park, H. Cho, S. Park, M. B. Shim, S. Jeon and D. Y. Chung, *Nat. Nanotechnol.*, 2012, **7**, 803.
- P. Lee, J. Ham, J. Lee, S. Hong, S. Han, Y. D. Suh, S. E. Lee, J. Yeo, S. S. Lee and D. Lee, *Adv. Funct. Mater.*, 2014, **24**, 5671.
- J. Y. Woo, K. K. Kim, J. Lee, J. T. Kim and C. S. Han, *Nanotechnology*, 2014, **25**, 285203.
- L. Hu, W. Yuan, P. Brochu, G. Gruner and Q. Pei, *Appl. Phys. Lett.*, 2009, **94**, 161108.
- F. Xu, W. Lu and Y. Zhu, *ACS Nano*, 2010, **5**, 672.
- Y. Zhu and F. Xu, *Adv. Mater.*, 2012, **24**, 1073.
- N. Bowden, S. Brittain, A. G. Evans, J. W. Hutchinson and G. M. Whitesides, *Nature*, 1998, **393**, 146.
- Y. Shang, X. He, Y. Li, L. Zhang, Z. Li, C. Ji, E. Shi, P. Li, K. Zhu and Q. Peng, *Adv. Mater.*, 2012, **24**, 2896.
- H. W. Liang, Q. F. Guan, L. T. Song, H. B. Yao, X. Lei and S. H. Yu, *NPG Asia Mater.*, 2012, **4**, e19.
- Z. Chen, W. Ren, L. Gao, B. Liu, S. Pei and H. M. Cheng, *Nat. Mater.*, 2011, **10**, 424.
- C. Yu, C. Masarapu, J. Rong, B. Wei and H. Jiang, *Adv. Mater.*, 2009, **21**, 4793–4797.
- C. Wu, L. Fang, X. Huang and P. Jiang, *ACS Appl. Mater. Interfaces*, 2014, **6**, 21026.

- 36 H. Wu, L. Hu, M. W. Rowell, D. Kong, J. J. Cha, J. R. McDonough, J. Zhu, Y. Yang, M. D. McGehee and Y. Cui, *Nano Lett.*, 2010, **10**, 4242.
- 37 Y. Zhang, C. Sheehan, J. Zhai, G. Zou, H. Luo, J. Xiong, Y. Zhu and Q. Jia, *Adv. Mater.*, 2010, **22**, 3027.
- 38 M. Chen, S. Duan, L. Zhang, Z. Wang and C. Li, *Chem. Commun.*, 2015, **51**, 3169.
- 39 Y. Yu, J. Zeng, C. Chen, Z. Xie, R. Guo, Z. Liu, X. Zhou, Y. Yang and Z. Zheng, *Adv. Mater.*, 2014, **26**, 810.
- 40 J. Park, S. Wang, M. Li, C. Ahn, J. K. Hyun, D. S. Kim, D. K. Kim, J. A. Rogers, Y. Huang and S. Jeon, *Nat. Commun.*, 2012, **3**, 916.
- 41 M. Chen, L. Zhang, S. Duan, S. Jing, H. Jiang and C. Li, *Adv. Funct. Mater.*, 2014, **24**, 7548.
- 42 X. Yu, B. Lu and Z. Xu, *Adv. Mater.*, 2014, **26**, 1044.
- 43 W. Wei, S. Yang, H. Zhou, I. Lieberwirth, X. Feng and K. Müllen, *Adv. Mater.*, 2013, **25**, 2909.
- 44 Y. Xu, K. Sheng, C. Li and G. Shi, *ACS Nano*, 2010, **4**, 4324.
- 45 F. Han, J. Li, S. Zhao, Y. Zhang, W. Huang, G. Zhang, R. Sun and C. P. Wong, *J. Mater. Chem. C*, 2017, **5**, 10167–10175.
- 46 Y. Song, D. Shan and E. Han, *Electrochim. Acta*, 2008, **53**, 2135.
- 47 X. Luo and T. Xuan, *Electroplat. Pollut. Control*, 2007, **27**, 8.
- 48 X. Gan, Y. Wu, L. Liu, B. Shen and W. Hu, *J. Alloys Compd.*, 2008, **455**, 308.
- 49 G. Krulik, *Othmer Encyclopedia of Chem. Technol.*, 2000.
- 50 H. Dai, H. Li and F. Wang, *Appl. Surf. Sci.*, 2006, **253**, 2474.
- 51 D. Goyal, T. Lane, P. Kinzie, C. Panichas, K. M. Chong and O. Villalobos, *Proc. 52nd ECTC*, 2002, p. 732.
- 52 M. Paunovic, *Proceedings of the Second Symposium on Electrochemically Deposited Thin Films*, Electrochemical Society, 1995.
- 53 B. Song, D. Li, W. Qi, M. Elstner, C. Fan and H. Fang, *ChemPhysChem*, 2010, **11**, 585.
- 54 C. W. Hsu, C. W. Li and G. J. Wang, *RSC Adv.*, 2014, **4**, 12127.
- 55 J. Nutting and J. Nuttall, *Gold Bull.*, 1977, **10**, 2.
- 56 Y. Y. Yang, Z. A. Hu, Z. Y. Zhang, F. H. Zhang, Y. J. Zhang, P. J. Liang, H. Y. Zhang and H. Y. Wu, *Mater. Chem. Phys.*, 2012, **133**, 363–368.
- 57 G. Marshall, D. Lewis and B. Dodds, *Surf. Coat. Technol.*, 1992, **53**, 223.
- 58 S. Newase and A. Bankar, *Bull. Mater. Sci.*, 2017, **40**, 157.